Journal of Catalysis **200,** 181–193 (2001)
doi:10.1006/jcat.2001.3201, available online at http://www.idealibrary.com on IDEAL®

Effects of the Nature of the Reducing Agent on the Transient Redox Behavior of NM/$Ce_{0.68}Zr_{0.32}O_2$ (NM = Pt, Pd, and Rh)

N. Hickey,* P. Fornasiero,* J. Kašpar,*,[1] J. M. Gatica,† and S. Bernal†

*Dipartimento di Scienze Chimiche, Università di Trieste, Via Giorgieri 1, 34127 Trieste, Italy; and †Departamento de Ciencia de los Materials e Ingeniería Metalúrgica y Química Inorgánica, Universidad de Cádiz, Apartado 40, Puerto Real, 11510, Spain

Received December 19, 2000; revised February 5, 2001; accepted February 5, 2001; published online April 18, 2001

The influence of reducing conditions on transient redox behavior of a series of noble metal (NM)-loaded $Ce_{0.68}Zr_{0.32}O_2$ and CeO_2 materials was investigated. When H_2 was used as a reducing agent, significant dynamic oxygen storage (H_2-OSC) values, with H_2O formation, were measured at room temperature (RT). This is attributed to H_2 spilled over the support followed by titration of this adsorbed hydrogen by O_2. The phenomenon requires the presence of metal to activate H_2, and was observed for Rh, Pd, and Pt, all of which show high efficiency in this regard. Furthermore, there appears to be a direct relationship between this process and surface area: Decreasing the surface area of samples diminishes RT H_2-OSC proportionally. The higher thermal stability of ceria–zirconia relative to ceria means that H_2-OSC remains significant even after severe redox aging. Over Pt/CeO_2, the H_2-OSC values measured at 373–773 K depend on surface area, indicating that the reduction is a surface-related process, whereas for ceria–zirconia-supported samples deeper reduction/vacancy creation becomes evident as the temperature is increased, the dynamic H_2-OSC being therefore independent of sample surface area. When CO is used as reducing agent, complicated dynamic CO-OSC behavior is observed, with surface reduction, CO storage, and CO desorption being detected. For the fresh (oxidized) high-surface-area Pt/$Ce_{0.68}Zr_{0.32}O_2$ catalyst, appreciable CO-OSC is detected only at and above 473 K. When the catalyst is prereduced at 500 K, CO-OSC is observed at 373 K. In contrast, no appreciable CO-OSC was detected over low-surface-area samples below 673 K. Compared with Pd and Pt, which exhibit similar behavior, the presence of Rh promotes support reduction by CO.

Key Words: **oxygen storage capacity; ceria–zirconia; redox properties; platinum; palladium; rhodium; three-way catalysts; hydrogen spillover; CO oxidation.**

1. INTRODUCTION

The ability of a three-way catalyst (TWC) to attenuate the negative effects of rich/lean oscillations in exhaust gas composition is a crucial factor in determining its overall efficiency (1, 2). It is generally accepted that the most important factor in this regard is the oxygen storage capacity (OSC): loss of OSC results in a severe loss of TWC efficiency (3). Accordingly, this has led to the development of on-board diagnostics (OBD) which, by *in situ* monitoring of the OSC, detects the failure of the catalytic converter. In modern TWC formulations, ceria–zirconia mixed oxides are included to cater for the OSC requirement, replacing CeO_2, which was used in earlier formulations (4). OSC is fundamentally related to redox behavior. Thus, a detailed knowledge of the redox properties of these materials is desirable with a view to designing improved TWCs.

OSC is usually discussed in terms of the ability of the catalyst to attenuate the effects of rich/lean excursions through the Ce^{3+}/Ce^{4+} redox couple:

$$CeO_2 \underset{H_2O/CO_2}{\overset{H_2/CO}{\longleftrightarrow}} CeO_{2-x} + x/2O_2.$$

Formation of vacancies is often either implied or assumed. However, in a recent communication, we demonstrated that, due to the phenomenon of hydrogen spillover, high OSC may be measured at room temperature (RT) over a 0.58% Pt/$Ce_{0.68}Zr_{0.32}O_2$ catalyst (5). This raises the possibility that spillover may also be a factor at higher temperatures of investigation. As H_2 is always present in exhaust gas composition in a ratio of 1 : 3 with respect to CO (1), this is a potentially important finding, worthy of further investigation.

OSC investigations may be divided into two categories: total OSC and dynamic OSC (2, 6). The former refers to O_2 uptake measured after a switch from a reducing to an oxidizing (O_2) atmosphere and involves single reduction and reoxidation steps; the latter refers to the O_2 uptake measured during continuous cycling between reducing and oxidizing (O_2) atmospheres. Two techniques are generally used in investigation of dynamic OSC. Following the

[1] To whom correspondence should be addressed. E-mail: kaspar@univ.trieste.it. Fax: +39 040 6763903.

0021-9517/01 $35.00

TABLE 1

Sample Summary

Sample composition	NM loading (wt%)	Sample designation	Surface area ($m^2 g^{-1}$)	Aging procedure[a] [gas, time (min), T (K)]
$Pt/Ce_{0.68}Zr_{0.32}O_2$ (HSA)	0.58	PtCeZr1	100	
		PtCeZr2	77	H_2, 5, 1173
		PtCeZr3	15	H_2, 480, 1273
		PtCeZr4	7	(1) H_2, 480, 1273, (2) H_2, 480, 1343
		PtCeZr5	30	Redox-aging (procedure B)
$Pt/Ce_{0.68}Zr_{0.32}O_2$ (LSA)	0.55	PtCeZr6	21	
Pt/CeO_2(HSA)	0.54	PtCe1	88	
		PtCe2	50	H_2, 30, 1013
		PtCe3	7	Redox-aging (procedure B)
Pt/CeO_2(LSA)	0.53	PtCe4	18	
Pt/γ-Al_2O_3	0.5	PtAl1	99	
$Pd/Ce_{0.68}Zr_{0.32}O_2$ (HSA)	0.64	PdCeZrl	85	
$Rh/Ce_{0.68}Zr_{0.32}O_2$ (HSA)	0.69	RhCeZrl	94	

[a] For samples of compositions 0.58% $Pt/Ce_{0.68}Zr_{0.32}O_2$ and 0.54% Pt/CeO_2, the HSA materials were used to obtain samples of lower surface area, by means of the aging procedures outlined. All pretreatments were conducted *ex situ*, except redox-aging (procedure B). All *ex situ* pretreatments in H_2 were conducted using a 5% H_2 in Ar mixture and at a flow rate of 20 ml min^{-1}. See Section 2 for details of procedure B.

pioneering work of Yao and Yu-Yao (2), dynamic OSC measurement involves alternately pulsing the chosen reducing agent (usually CO but sometimes H_2) and O_2 over the material under investigation. More recently, the OBC technique has been developed by Bernal *et al*. (7). In this method O_2 is pulsed over the sample in a flow of inert gas, which effectively corresponds to oscillations between mildly reducing and oxidizing conditions.

Relative to ceria, ceria–zirconia mixed oxides are generally believed to show better redox properties and, therefore, enhanced OSC. Likewise, the zirconium-doped cerium oxides exhibit higher thermal stability, thus showing enhanced resistance against the deactivation effects induced by high-temperature aging processes (4). Improved redox behavior of fresh and aged ceria–zirconia materials has been demonstrated by temperature-programmed reduction (TPR), and has been suggested to be a function of the structural properties of these supports (8, 9). However, less attention has been devoted to dynamic redox behavior and to the effect of the supported metal thereon (10, 11). In addition, to our knowledge, the influence of the reducing agent employed has not been considered for noble metal (NM) ceria–zirconia mixed oxides. In the light of our previous communication (5), the role played by hydrogen spillover in OSC determinations is another important consideration within this framework. In the present work, the effect of the reducing agent, H_2 or CO, on the total and dynamic OSC of a series of NM-loaded $Ce_{0.68}Zr_{0.32}O_2$ catalysts is investigated and a comparison with results obtained using Pt/CeO_2 and Pt/Al_2O_3 is made.

2. EXPERIMENTAL

2.1. Catalyst Preparation and Pretreatment Procedures

Pt-, Pd-, and Rh-loaded $Ce_{0.68}Zr_{0.32}O_2$ and Pt/CeO_2 were prepared and supplied by Rhodia as part of the CEZIRENCAT network.[2] The noble metals were impregnated onto the support using $Rh(NO_3)_3$, $Pt[(NH_3)_4](NO_3)_2$, and $Pd[(NH_3)_4](NO_3)_2$ as precursors. The high- and low-surface-area $Ce_{0.68}Zr_{0.32}O_2$ (HSA, 100 $m^2 g^{-1}$; LSA, 21 $m^2 g^{-1}$) and CeO_2 (HSA, ~100 $m^2 g^{-1}$; LSA, 18 $m^2 g^{-1}$) were from a previous study (12). Pt/γ-Al_2O_3 was prepared by wet impregnating $Pt(NH_3)_2(NO_2)_2$ on γ-Al_2O_3 (Alfa products). This sample was dried overnight at 383 K and then calcined for 5 h at 773 K.

To investigate the effect of surface area, in addition to the starting HSA and LSA catalysts, two types of treatments, i.e., *ex situ* reduction and *in situ* procedure B outlined below, were applied to HSA $Pt/Ce_{0.68}Zr_{0.32}O_2$ and Pt/CeO_2 to obtain samples with lower surface areas. Table 1 summarizes the samples used.

For each OSC measurement, the sample under investigation was subjected to one of four *in situ* pretreatment procedures:

A. *Cleaning*: This procedure was always applied as a first step. It consisted of heating the sample in 5% O_2/Ar

[2] The CEZIRENCAT Project is a multilaboratory project in the area of three-way catalysis funded by the European Union. Home page: http://www.dsch.univ.trieste.it/cezirencat/index.html.

(25 ml min^{-1}) from RT to 823 K at a heating rate of 10 K min^{-1}, holding at that temperature for 1 h, and then cooling slowly, first in O_2/Ar to 373 K and finally to RT in Ar (60 ml min^{-1}). The aim of this treatment was to reproducibly obtain an oxidized, clean sample surface (13).

B. *Redox-aging*: Pretreatment A was followed by (i) reduction to 1273 K at 10 K min^{-1} followed by isothermal reduction at 1273 K for 15 min (5% H_2 in Ar, 25 ml min^{-1}); (ii) flushing at 1273 K for 15 min and slow cooling to 700 K (in Ar); (iii) reoxidation at 700 K for 30 min and cooling to 423 K (in 5% O_2 in Ar); and (iv) cooling in Ar to RT. Unless otherwise stated, a flow rate of 60 ml min^{-1} was used.

C. *Reduction*: A cleaned sample was heated in 5% H_2 in Ar to 500 K (10 K min^{-1}), maintained at 500 K for 1 h, and cooled slowly to RT; the flow was then switched to Ar at RT (30 min, 25 ml min^{-1}).

D. *Reduction/passivation*: A reduced sample was treated with pulses of O_2 (500 μl) at RT for 1 h. Such a passivation procedure leads to almost full reoxidation of the support (14).

2.2. Hydrogen Chemisorption and BET Surface Area Measurements

H_2 chemisorption and BET surface area measurements were conducted using a Micromeritics ASAP 2000 analyzer. H_2 chemisorption was measured at 308 and 193 K, as fully described previously (15, 16). Typically, 1.0 g of catalyst was used and the samples were prereduced at 500 K for 2 h. Two values of adsorbed volumes are reported. The first was determined by extrapolation to zero pressure of the linear part of the adsorption isotherm (4–20 Torr). Apparent dispersions were calculated from these values, assuming a H : NM chemisorption stoichiometry of 1 : 1. In addition, the values of total H_2 chemisorbed at the final adsorption pressure (20 Torr) are reported. BET surface area measurements were carried out on the same instrument.

2.3. Temperature-Programmed Reduction

Temperature-programmed reduction experiments were conducted using a VG Sensorlab quadropole mass spectrometer (TPR/MS) with POSTSOFT analysis software, as reported previously (15). The TPR/MS of the cleaned sample was obtained according to pretreatment procedure B. After this, the TPR/MS profile of the redox-cycled sample was collected in the same way. The degree of reduction attained during TPR was estimated in separate experiments using a thermal conductivity detector (TCD). Using identical flow conditions but ca. 0.05 g of catalyst, procedure B was followed until the reoxidation step, at which point O_2 uptake was quantified by a pulse technique to ensure full oxidation in the bulk of the solid solution (17).

2.4. Dynamic OSC Measurements

After sample pretreatment (A–D), analysis was performed by increasing the temperature of the catalyst (0.020 g, maintained in a flow of Ar of 25 ml min^{-1}) in a stepwise manner and, during the isothermal steps (30 min), alternately pulsing reductant (H_2 (H_2-OSC) or CO (CO-OSC)) and O_2 over the sample every 70 s. The temperature range RT to 773 K was investigated. The reducing agent was always pulsed first. For H_2-OSC measurements, loop volumes of 500 μl (22.3 μmol) and 250 μl (11.2 μmol) were used for H_2 and O_2, respectively; while for CO-OSC measurements, loop volumes of 100 μl (4.5 μmol) were used for both CO and O_2. A thermal conductivity detector was used for quantification of H_2, CO, O_2, and CO_2. Following the definition of Yao and Yu Yao (2), OSC was measured as the uptake of O_2 from the O_2 pulse. All values quoted are the average values obtained once the system exhibited steady-state behavior. To avoid changes in the contact times, constant loop volume and sample weight were kept through the series of experiments. This resulted in full CO uptake in some of the experiments. When H_2 was used as the reducing agent, a molecular sieve trap was used to remove water from the gas stream; when CO was used, the evolved CO and CO_2 were separated on a Porapak Q column. A mass spectrometer (MS) was used for supporting qualitative information using the following conditions: 0.200 g sample, 25 ml min^{-1} Ar, loop volume of 1 ml (44.6 μmol). The experimental setup differed in these experiments in that, although heated, longer transfer lines were necessary. To account for the increased tailing of peaks that resulted, pulses were made at 100-s intervals.

3. RESULTS

3.1. H_2 Chemisorption and Surface Area Measurements

The results of surface area analysis and H_2 chemisorption of the samples investigated are presented in Tables 1 and 2 respectively. All of the HSA materials investigated exhibit similar high surface area (85–100 m^2 g^{-1}). Of the data available, chemisorption measurements at 193 K indicate that these samples also have similar dispersions. It should be noted that spillover is arrested at this temperature (16, 18). The well-established problem of hydride formation prevented a similar analysis in the case of the Pd/CeZr1 sample. Chemisorption measurements at 298 K indicate that the ceria-based samples exhibit high spillover and accumulation of H_2 over the support while PtAl1 does not. In fact, the near equality of the data obtained at 193 and 298 K indicates negligible amounts of hydrogen spilled over the support for this sample. Furthermore, there is a significantly higher uptake for the PtCeZr samples rela-

TABLE 2

Volumetric H_2 Chemisorption

	H_2 chemisorption[a]						
	193 K			298 K			
Sample	Uptake at 0 Torr (ml g^{-1})	Uptake at 20 Torr (ml g^{-1})	H/NM[b]	Uptake at 0 Torr (ml g^{-1})	Uptake at 20 Torr (ml g^{-1})	H/NM[b]	Normalized uptake[c] (H atoms nm^{-2})
PtCeZr1	0.31	0.37	0.94	6.78	7.09	20.3	3.5
PtCe1	0.30	0.31	0.98	3.88	4.02	12.3	2.2
PtAl1	0.26	0.27	0.89	0.28	0.30	0.98	0
PdCeZr1	—	—	—	5.94	6.30	11.3	3.5
RhCeZr1	0.52	0.62	0.69	6.50	6.81	12.0	3.5
PtCeZr2	—	—	—	5.31	5.56	16.8	
PtCeZr3	0.02	0.02	0.10	0.98	1.04	3.15	3.5
PtCeZr4	—	—	—	0.90	0.99	2.90	
PtCeZr5	0.09	0.09	0.26	1.40	1.61	4.20	2.4
PtCeZr6	0.27	0.29	0.85	1.64	1.74	5.20	3.7
PtCe2	0.11	0.11	0.38	2.74	2.81	5.00	2.9
PtCe3	0.04	0.04	0.11	0.47	0.49	1.50	3.4

[a] Sample were first cleaned according to pretreatment A (see text) and then reduced at 500 K for 1 h, followed by evacuation at 673 K for 4 h. The H_2 pressure range 2–20 Torr was employed. Adsorbed volumes were determined by extrapolation to zero pressure of the linear part of the adsorption isotherm (0 Torr). Cumulative H_2 adsorption at P = 20 Torr is also given.

[b] H/NM calculated at 0 Torr. As shown previously, under our experimental conditions, at 193 K only H adsorbed on NM is detected, while at 298 K a contribution of spilled over H is also present.

[c] Number of hydrogen atoms adsorbed on the support at 0 Torr/nm^2 calculated as (H atoms adsorbed at 298 K − H atoms adsorbed at 193 K)/(BET surface area − NM exposed surface area). H/Pd = 1 was assumed due to unavailability of low-temperature chemisorption data.

tive to PtCe, indicating the key role of the added ZrO_2 in promotion of H_2 spilling/adsorption over the CeO_2-containing support (compare Fig. 3b below). When normalized as a coverage of H atoms per square nanometer of support, the H_2 uptake values are very similar for the three cleaned NMCeZr samples. The magnitude of the contribution from metal-adsorbed hydrogen was estimated from the data at 193 K (16, 18). The normalized H_2 uptake is somewhat lower for the redox-aged PtCeZr5 compared with other NMCeZr samples. The sensitivity of spillover phenomena to pretreatment is well known and could account for this exception.

Aging of the PtCeZr1, PtCe1, and PtAl1 samples decreases surface areas. The higher thermal stability of ceria–zirconia is illustrated by the smaller decrease in the surface area of PtCeZr1 compared with PtCe1 when the same redox-aging procedures (B) are applied to both to yield PtCeZr5 (30 m^2 g^{-1}) and PtCe3 (7 m^2 g^{-1}), respectively (Table 1). Reduction at 1343 K was necessary to achieve a surface area of 7 m^2 g^{-1} in the PtCeZr1 sample. Aging also decreases the H/Pt values at both 298 and 193 K. However, with few exceptions, the H-atom coverage at 298 K per square nanometer is relatively constant, suggesting that, under the present experimental conditions, the mechanism of H_2 spilling and adsorption over the support is not strongly affected by the severity of the pretreatments.

3.2. Temperature-Programmed Reduction

H_2 TPR/MS profiles of the cleaned (pretreatment A) and redox-aged (pretreatment B) NMCeZr are shown in Fig. 1. The overall TPR behavior of the cleaned samples is consistent with previous results of TPR investigations of such materials (19). All of the samples exhibit a dominant low-temperature reduction feature. In the cases of PdCeZr1 and RhCeZr1, this is attributed to an initial reduction of supported NM oxide, which in turn results in support reduction through spillover of hydrogen species. TPR of a Pd/ZrO_2 sample prepared in the same way as the present samples (not shown) indicates that the Pd is in fact reduced at RT, as negligible uptake was observed during the temperature ramp. This suggests that the H_2 uptake observed for PdCeZr1 can be attributed to support reduction. For cleaned PtCeZr1, reduction takes place at higher temperature, which is due to the comparative difficulty of the reduction of the surface platinum oxide (20).

H_2 uptake is always followed by the appearance of H_2O, indicating that either adsorption effects are in operation and/or H_2 activation (i.e., the so-called reversible reduction (21)) precedes the irreversible reduction (i.e., oxygen vacancy creation with H_2O formation). The term *reversible reduction* was introduced to describe the ability of Rh/CeO_2

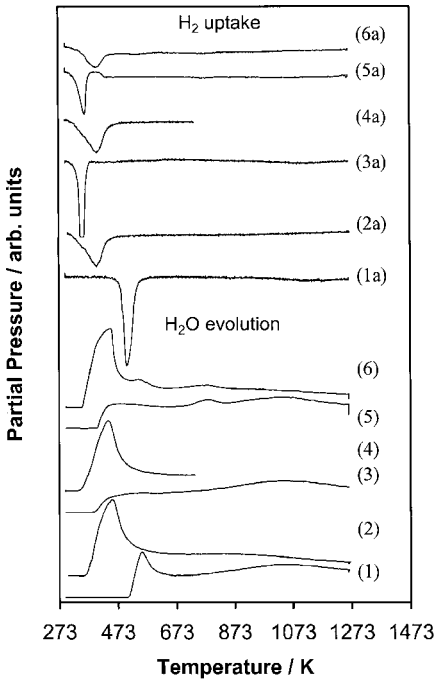

FIG. 1. H_2 uptake (a traces) and H_2O evolution observed during TPR/MS profiles of (1) cleaned Pt/$Ce_{0.68}Zr_{0.32}O_2$, (2) redox-aged Pt/$Ce_{0.68}Zr_{0.32}O_2$, (3) cleaned Rh/$Ce_{0.68}Zr_{0.32}O_2$, (4) redox-aged Rh/$Ce_{0.68}Zr_{0.32}O_2$, (5) cleaned Pd/$Ce_{0.68}Zr_{0.32}O_2$, and (6) redox-aged Pd/$Ce_{0.68}Zr_{0.32}O_2$.

to adsorb and spill H_2 over CeO_2, leading to Ce^{4+} reduction. In analogy with chemisorption experiments, this process is termed reversible since Ce^{3+} can be reoxidized by a simple evacuation, i.e., in the absence of an oxidizing agent (21). On the contrary, the term *irreversible reduction* was employed because the presence of an oxidizing agent, such as O_2, CO_2, NO, or H_2O, is necessary to recover the initial Ce(IV) state when oxygen vacancies have been created in the reduction. The H_2O profiles indicate that there are high-temperature regions of reduction. H_2O detection has not ceased by the end of the experiment and the profiles are not symmetrical. Factors such as H_2O retention on the transfer lines, change in signal baseline due to the process of sintering, and the large amount of sample used could also contribute to these observations.

The effects of redox-aging are also typical of the behavior of these material after such treatments (19). In the case of PtCeZr1, all features are moved to lower temperatures. The most likely explanation of this is that the reoxidation procedure does not fully oxidize the metal. If so, the resulting partly oxidized platinum would be more easily reduced, thus favoring the occurrence of hydrogen spillover, which in turn would allow the support reduction to start at a lower temperature. For PdCeZr1 and RhCeZr1, redox cycling results in the observation of H_2O evolution at lower temperatures, while H_2 uptake commences immediately, as for the cleaned samples, but takes place over a broader range of temperatures.

In pulsed reoxidation experiments, an O_2 uptake (total-OSC) of ca. 20 ml g^{-1} was obtained for all the profiles included in Fig. 1. For the purposes of comparison, it should be noted that an O_2 uptake of 17 ml O_2 g^{-1} was measured for the PtCe1 sample in identical experiments.

3.3. Dynamic OSC Using H_2 as Reducing Agent

The results of dynamic H_2-OSC measurements on the reduced (pretreatment C) and redox-aged (pretreatment B) samples are reported in Table 3. Close to stoichiometric O_2/H_2 uptakes were measured in all the experiments, including those at RT. Accordingly only O_2 uptake is reported. High dynamic H_2-OSC values are measured over all the samples, the highest being those measured at 773 K over the redox-aged NM/CeZr samples, which correspond to about half of the total OSC measured after the TPR experiments. Both Pd- and Pt-loaded CeZr samples show very similar values, independently of the pretreatment, suggesting that mostly the nature of the support affects the dynamic H_2-OSC here measured. Notably, a constant, or even slightly decreasing, H_2-OSC is measured in the PtCe1, which drops after redox-aging. Very low H_2-OSC is measured over PtAl1, which is in line with the observation that the redox reaction occurs at the support.

A remarkable finding reported in Table 3 was the high OSC measured at RT. To ensure the lack of artifacts, the issue of water formation at RT was addressed by mass spectrometry. Figure 2 contains the results of dynamic H_2-OSC investigations using PtCeZr1 and PtAl1 after various pretreatments. When observed, H_2O is produced continuously, with minor perturbations coinciding with H_2 or O_2 pulses. This indicates the occurrence of H_2O adsorption effects on the surface of the catalysts and maybe, to some extent, on the transfer line. Accurate quantification was therefore not possible. Significant H_2O formation, in conjunction with H_2 and O_2 uptake, is observed only for the ceria–zirconia-based sample after reduction or reduction/passivation (pretreatments C and D) or redox cycling (pretreatment B). By contrast, very low consumption of reactants and formation of H_2O was observed for both the reduced PtAl1 and cleaned PtCeZr1 samples. An analogous series of experiments (not shown) confirmed water formation with reduced and, to a much smaller extent, redox-aged PtCe1 at RT. Individual pulses resulted in catalyst bed temperature increases of the sample of 5–6 K above RT in the case of PtCeZr1 sample and 2–3 K in the case of PtCe1.

Dynamic H_2-OSC measurements were also conducted at RT over samples of composition 0.58% Pt/$Ce_{0.68}Zr_{0.32}O_2$ and 0.54% Pt/CeO_2 with lower surface areas, in order to verify the possible link between these properties. These results are summarized in Fig. 3a. CeO_2 is

TABLE 3

Effect of Surface Area on Dynamic H_2-OSC Measurements Using H_2 as Reducing Agent

Sample	Surface area ($m^2 g^{-1}$)	Pretreatment[a]	H_2-OSC at various temperatures[b,c] ($ml\ O_2\ g^{-1}_{catalyst}$) RT	373 K	473 K	573 K	673 K	773 K
PtCeZr1	100	Reduction	6.3	7.1	7.5	7.6	8.1	8.9
PtCeZr5	30	Redox-aging	2.8	4.1	9.1	8.7	9.8	11.6
PtCeZr6	21	Reduction	1.5	2.0	4.4	5.0	5.9	6.8
PtCe1	88	Reduction	4.2	4.5	4.4	4.1	3.6	3.4
PtCe4	18	Reduction	1.4	1.6	1.5	1.5	1.3	1.3
PtCe3	7	Redox-aging	0.6	0.9	0.9	0.8	0.9	1.0
PdCeZr1	85	Reduction	6.2	7.1	7.4	7.7	8.3	8.8
PdCeZr1	—	Redox-aging	2.5	3.6	7.9	8.8	9.7	10.6
RhCeZr1	94	Reduction	2.4	6.5	7.7	8.0	8.6	9.0
RhCeZr1	—	Redox-aging	0.7	4.0	8.0	8.7	9.6	10.6
PtAl + CeZr[d]	—	Reduction	2.0	4.4	6.5	7.9	9.2	8.9
CeZr[e]	100	Cleaning	0.0	0.0	0.0	0.0	0.6	2.1

[a] See Section 2 for details of pretreatment procedures. Cleaning = procedure A. Redox-aging = procedure B. Reduction = procedure C.

[b] OSC values are given as ml O_2 uptake g^{-1}. Estimate of the upper limit of the contribution of NM oxide reduction to the H_2-OSC calculated fom NM metal loading reported in Table 1 indicates contributions of 0.3, 0.7, and 1.1 ml $O_2\ g^{-1}_{catalyst}$ for Pt, Pd, and Rh, respectively.

[c] OSC measurements over PtAl1 showed no value greater than 0.2 ml g^{-1} at RT to 773 K.

[d] Physical mixture of equal amounts of PtAl1 and HSA $Ce_{0.68}Zr_{0.32}O_2$.

[e] HSA $Ce_{0.68}Zr_{0.32}O_2$.

known to easily sinter under reducing conditions (22). Accordingly, we progressively increased the reduction temperature of the catalysts, leading to lower surface areas (Table 1). It should, however, be noted that high-temperature reduction also can lead to other phenomena such as NM sintering, metal particle decoration, and encapsulation, in addition to support sintering (23). Two samples, PtCeZr6 and PtCe4, containing LSA $Ce_{0.68}Zr_{0.32}O_2$ (21 $m^2\ g^{-1}$) and CeO_2 (18 $m^2\ g^{-1}$) were therefore investigated. These yielded RT dynamic H_2-OSC values of 1.5 and 1.4 ml $O_2\ g^{-1}$, respectively. Here, the above-quoted phenomena are absent, since the samples were prepared by first sintering the support at 1173 K and then loading the metal. Thus, within experimental error, there appears to be a linear relationship between the RT H_2-OSC and the surface area for both the CeZr and CeO_2 samples, and this relationship appears to be largely independent of the nature of the pretreatment (i.e., reduction or redox-aging). Notably, a significantly higher slope was detected for the ceria–zirconia series compared with the ceria series. For comparison, H_2 chemisorption at 298 K is plotted versus BET surface in Fig. 3b, showing the same kind of trends as observed in the dynamic OSC measured at RT.

On increasing the temperature of dynamic investigation, the correlation between surface area and dynamic OSC behavior is no longer apparent (Table 3). Thus, the values obtained for the PtCeZr5 sample lie above those of the other PtCeZr samples investigated for temperatures higher then 473 K. In fact, no clear pattern emerges at higher temperatures, other than the observation that differences between the samples become smaller, indicating that other factors, such as preparation and structure, become important in the behavior observed. Finally, comparison of the data obtained on RhCeZr1 with those obtained on PdCeZr1 and PtCeZr1 catalysts shows that under our dynamic OSC conditions, Rh is less effective after an equivalent pretreatment in promoting RT H_2-OSC compared with the other two NMs, while at higher temperatures similar H_2-OSC values are measured.

3.4. Dynamic OSC Using CO as Reducing Agent

The results of analogous dynamic CO-OSC measurements on PtCeZr1 after pretreatment C (reduction) are summarized in Fig. 4a. The corresponding sequence of pulses is shown in Fig. 4b. The complex behavior observed when CO-OSC is measured over a reduced surface is partially illustrated in this figure. Both O_2 and CO pulses show a transient type of behavior between RT and 473 K, while above this temperature the pulses show a constant steady-state behavior at a constant temperature. Appreciable CO_2 formation was detected at temperatures $\geq$ 473 K. The initial pulses at 373 K also showed some CO_2 production. In addition to the sample reduction indicated by the appearance of CO_2 at and above 473 K, it is clear

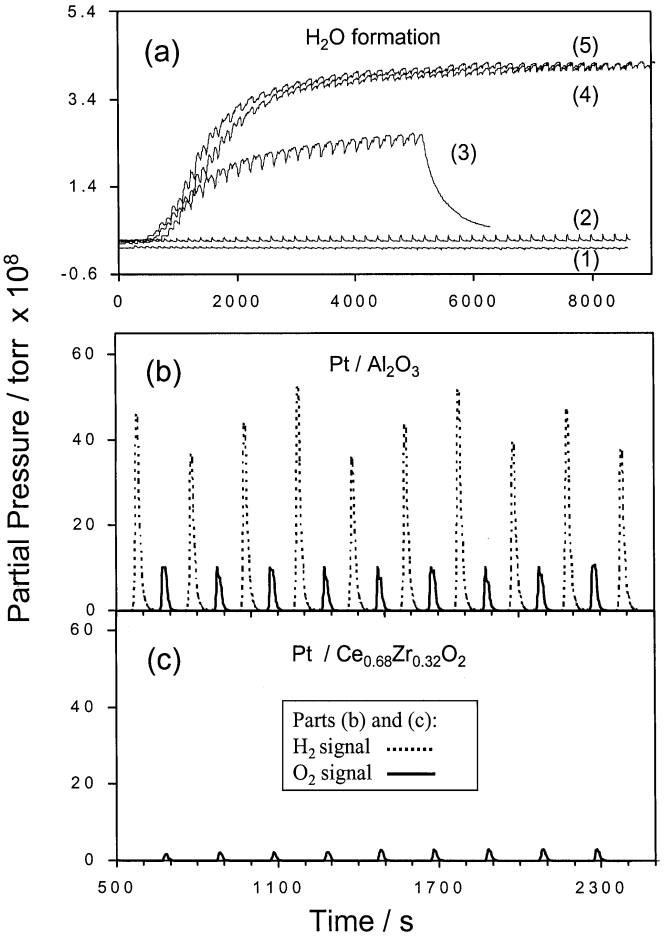

FIG. 2. Dynamic H_2-OSC measured at RT using mass spectrometry detection: (a) H_2O production (m/e = 18) over (1) reduced Pt/Al_2O_3, (2) cleaned Pt/$Ce_{0.68}Zr_{0.32}O_2$ (for clarity this trace is displaced), (3) redox cycled Pt/$Ce_{0.68}Zr_{0.32}O_2$, reaction stopped at 5000 s, (4) reduced/passivated by O_2 pulses at RT Pt/$Ce_{0.68}Zr_{0.32}O_2$, and (5) reduced Pt/$Ce_{0.68}Zr_{0.32}O_2$. (b) H_2 (m/e = 2) and O_2 (m/e = 32) over reduced Pt/Al_2O_3. (c) H_2 (m/e = 2) and O_2 (m/e = 32) over reduced Pt/$Ce_{0.68}Zr_{0.32}O_2$. MS was tuned to enhance the sensitivity toward H_2. Samples of 200 mg and loop volumes of 1 ml were employed. Samples reduced at 500 K (5% H_2 in He, 25 ml min^{-1}).

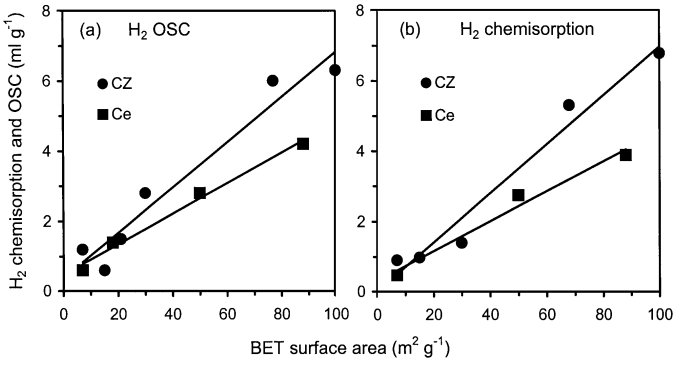

FIG. 3. Effects of BET surface on (a) the dynamic H_2-OSC measured at RT and (b) H_2 chemisorption at 298 K, for samples of compositions Pt/$Ce_{0.68}Zr_{0.32}O_2$ (CZ) and Pt/CeO_2 (Ce). Catalysts used are reported in Table 1. The lines are only as a visual guide.

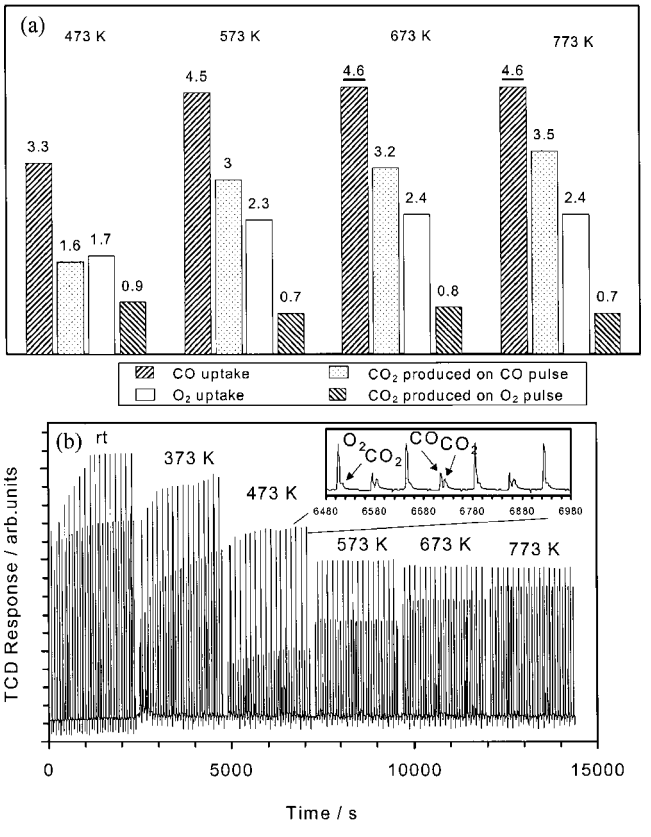

FIG. 4. (a) Dynamic CO-OSC measurements over reduced Pt/$Ce_{0.68}Zr_{0.32}O_2$ at various temperatures. The values shown are ml g^{-1} CO, O_2, and CO_2. Underlined values indicate full CO uptake in the experiment and therefore do not represent the full dynamic CO-OSC (see text). Standard deviation, ±0.4 ml g^{-1}. (b) Typical pulse sequence observed in (a). Experiments were performed by successively pulsing CO followed by pulse of O_2. Loops of 100 μl were used. Apparent maximum in CO uptake at 473 K is due to the increasing magnitude of the CO_2 peak, which becomes larger than the CO peak above this temperature (compare text inset).

that other pathways are available to CO. Up to 473 K, several pulses are required before the system exhibits a reproducible response, which could be associated with CO dissociation/disproportionation on the reduced $Ce_{0.68}Zr_{0.32}O_2$ surfaces (24–26), as this phenomenon was minimal for oxidized samples. It should be noted that under the present experimental conditions one O_2 pulse would be sufficient to remove all eventually spilled H species, possibly present after reduction. All the data shown in Fig. 4a refer to the final pulses, when the system exhibits a steady response at most temperatures. In addition, the phenomenon of CO storage and its subsequent oxidation to CO_2 is suggested by the appearance of CO_2 with the O_2 pulses in early pulses at 373 K and at higher temperatures (see inset to Fig. 4b). Storage effects are also indicated by the desorption

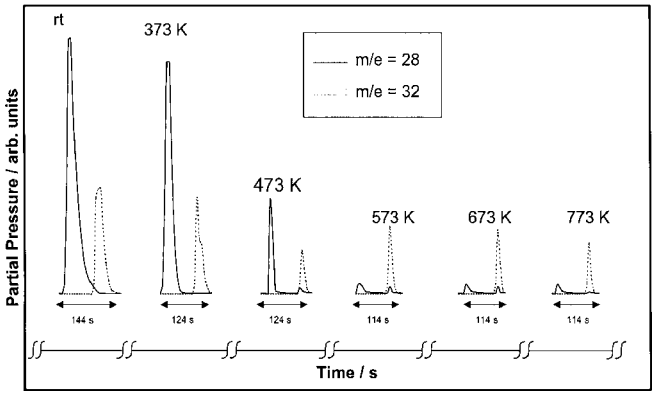

FIG. 5. Examples of traces observed for ($m/e = 32$) and ($m/e = 28$) for single CO/O_2 pulse cycles at various temperatures during dynamic CO-OSC measurements over cleaned $Pt/Ce_{0.68}Zr_{0.32}O_2$ (sample PtCeZr1). Where necessary, the ($m/e = 28$) traces have been corrected to account for contributions from CO_2 formation.

peak observed when the temperature was increased between the RT and 373 K sequences of pulses (Fig. 4b). The above-mentioned phenomenon of CO disproportionation to give CO_2 and adsorbed C, which can subsequently be oxidized to CO_2, may contribute to the CO_2 observed with the O_2 pulse. A further complication is the observation in the present work that CO may desorb along with the O_2 pulse. Figure 5 shows examples of CO and O_2 pulse cycles ($m/e =$ 28 and 32) made during dynamic CO-OSC measurements performed on cleaned PtCeZr1 from RT to 773 K. The $m/e = 28$ profile has been adjusted to eliminate contributions from CO_2 ($m/e = 44$). It is clear form this figure that starting from 473 K, CO desorbs during O_2 pulses. This represents a potential problem as the Porapak Q column, which is routinely used to separate O_2 and CO_2, could not separate O_2 and CO. Any CO desorption with the O_2 pulse would therefore tend to decrease the OSC measured using a TCD. Finally, as suggested by a referee, a possible contribution to the present phenomena could arise from the occurrence of water gas shift reaction at the expense of surface OH groups (27, 28). However, it should be recalled that the reported CO-OSC data correspond to the catalyst samples after reaching a steady-state reproducible behavior. Since the suggested process implies OH consumption, and the successive CO/O_2 pulses do not provide any way of regenerating the consumed OH, the relative weight of this process, if relevant, should progressively decrease as the number of alternated CO/O_2 pulses is increased.

All of this makes it difficult to separate the processes occurring with certainty. In view of this, consideration of mass balance becomes an important factor in analysis of the results obtained, as it can offer insight into the magnitude of these effects.

Table 4 contains the results of C and O mass balance considerations of the data obtained on the PtCeZr1 sample. These are designated δC and δO, and are defined as follows:

$$\delta C = (\text{CO uptake}) - (CO_2 \text{ produced}),$$

$$\delta O = (\text{“O” uptake from CO consumed (CO : O = 1 : 1 stoichiometry)}) + \text{apparent “O” uptake from } O_2) - (\text{total “O” produced as } CO_2).$$

The values calculated are expressed as milliliters per gram of catalyst. These calculations offer a method to establish whether the previously discussed phenomenon of CO storage and release as CO is a significant factor. For the cleaned and redox cycled materials, the mass balance is generally

TABLE 4

Effects of Pretreatments of $Pt/Ce_{0.68}Zr_{0.32}O_2$ on the Dynamic CO-OSC and Calculated Mass Balance in the Experiments: Sample PtCeZr1

Pretreatment	Parameter measured[a]	CO-OSC[b]/mass balance (ml g^{-1})				
		373 K	473 K	573 K	673 K	773 K
Cleaning	CO-OSC	0.0	1.1	**2.1**	**2.2**	**2.3**
	δC	0.3	0.1	0.7	<0.1	<0.1
	δO	0.3	0.5	1.2	0.6	0.4
Reduction	CO-OSC	0.7	1.7	**2.3**	**2.4**	**2.4**
	δC	0.9	0.8	0.7	0.6	0.5
	δO	1.8	1.6	1.5	1.4	1.1
Redox-aging	CO-OSC	0.0	0.1	0.7	**3.3**	**3.4**
	δC	0.1	0.3	0.2	0.5	0.3
	δO	0.1	0.5	0.3	0.8	0.4

[a] CO-OSC measured as O_2 uptake (ml g^{-1}). See text for the explanation of δC and δO. Standard deviation = 0.4 ml g^{-1}.

[b] OSC values in boldface were recorded with full uptake of CO and therefore do not represent the true dynamic CO-OSC at these temperatures, the amount of CO being a limiting factor.

good above 573 K and can be attributed to the error of the technique. However, on reduced PtCeZr1 the CO storage effects are significant, even at higher temperatures, indicating the importance of the pretreatment procedure to CO uptake and conversion.

The results of dynamic OSC measurements using CO as the reducing agent are summarized in Fig. 6. With respect to the effect of pretreatment, some differences are evident between the cleaned (pretreatment A) and reduced (pretreatment C) samples, mainly at 373 and 473 K. For the reduced sample, CO_2 production and O_2 uptake are evident at 373 K, which is lower than for the cleaned sample (473 K). At 573 K, the behavior observed is comparable for the two samples. At such temperatures, the O_2 pulses clean the sample and the CO can reduce the metal *in situ*, which would tend to equalize the states of the cleaned and reduced materials. This experiment confirms that also for CO activation, as a reducing agent under transient conditions, the presence of Pt metal or easily reducible metal species is essential to obtaining low-temperature dynamic OSC. In comparison with the behavior observed using H_2 as the reducing agent (TPR experiment; and the fact that cleaned PtCeZr1 showed no H_2-OSC up to 473 K), it is of interest to note that CO_2 production, indicating surface reduction, is observed at somewhat lower temperatures in the case of the cleaned sample. Thus, it appears that CO cause some surface reduction at lower temperatures than H_2. The effect of surface area on CO-OSC is shown in Fig. 6b. In general, decreasing the surface area results in an increase in the temperature at which OSC behavior is observed. In fact, only PtCeZr1 (100 $m^2\ g^{-1}$) shows appreciable activity at $\leq$ 573 K. Once significant OSC is detected, PtCeZr4 (7 $m^2 g^{-1}$) exhibits the poorest OSC behavior. The 15 and 30 $m^2 g^{-1}$ samples (respectively PtCeZr3 and PtCeZr5) exhibit comparable behavior; however, this could be accounted for by the different aging procedures employed for their preparation. This suggests that the extent of surface area is not the only relevant factor for CO-OSC at 673 K. The decrease in surface area eliminates the CO storage effects: no CO_2 was detected along with the O_2 pulses at any temperature. The effect of the NM was compared on samples after treatment B (Fig. 6c). The samples containing Pd and Pt exhibit similar behavior, whereas much higher dynamic OSC behavior is observed for the sample containing Rh. The ability of Rh to form *gem*-dicarbonyl species by reaction with surface OH groups in the presence of CO (29) could be a determining factor in this observation.

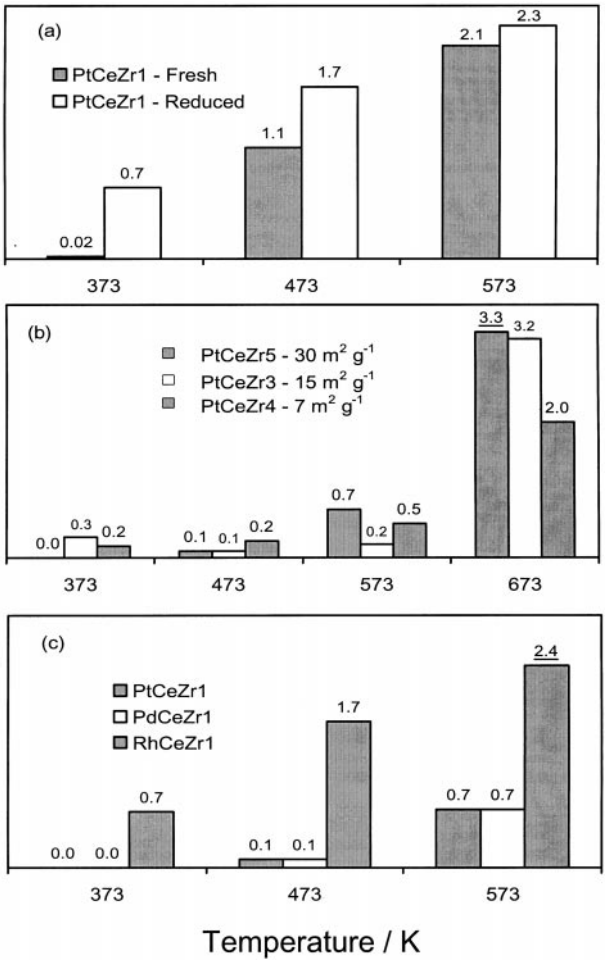

FIG. 6. Summary of dynamic CO-OSC measurements carried out on NM/$Ce_{0.68}Zr_{0.32}O_2$. Effects of (a) sample pretreatment in Pt/$Ce_{0.68}Zr_{0.32}O_2$, (b) $Ce_{0.68}Zr_{0.32}O_2$ surface area in Pt/$Ce_{0.68}Zr_{0.32}O_2$, and (c) nature of the noble metal in redox-aged NM/$Ce_{0.68}Zr_{0.32}O_2$ (NM = Pt, Rd, and Rh). Underlined values indicate full CO uptake and therefore do not represent the full dynamic CO-OSC (see text). Standard deviation, $\pm$0.4 ml $O_2\ g^{-1}$.

4. DISCUSSION

A major finding of the present is work is the high sensitivity to the nature of the reducing agent of the redox properties of the NM/$Ce_{0.68}Zr_{0.32}O_2$ system under transient conditions. The major results can be summarized as follows: (i) using H_2 as the reducing agent, very high dynamic OSC may be measured provided that noble metal or easily reducible metal species are present. The mechanism of this H_2-OSC, however, depends on temperature as there is a dependence on NM/$Ce_{0.68}Zr_{0.32}O_2$ surface area at low temperatures that is no longer apparent at high temperatures; (ii) CO-OSC is strongly affected by the sample pretreatment, significant storage effects being detected on a reduced $Ce_{0.68}Zr_{0.32}O_2$ surface; (iii) CO-OSC is detected only above 473 K and it is surface area dependent.

4.1. Mechanism of H_2-OSC

4.1.1. Room-temperature H_2-OSC. As outlined in our previous communication (5), we suggest the origin of

the high RT H_2-OSC is the same as that of the changes observed in the TPR profiles; i.e., the pretreatment procedures result either in Pt metal or a surface oxidized Pt metal, thereby facilitating spillover at RT. At RT, formation of oxygen vacancies in CeO_2-containing materials is unlikely. Accordingly we can depict the H_2-OSC as follows: Following the H_2 pulse, H_2 is chemisorbed on the metal and spilled over $Ce_{0.68}Zr_{0.32}O_2$, leading to reversible Ce(IV) reduction, as has been proposed for NM/CeO_2 (21). This spilled hydrogen is then released by the support when it is titrated by the following O_2 pulse leading to water formation. Removal of spilled hydrogen would then result in reoxidation of the support.

The low H_2-OSC value exhibited by PtAl1 demonstrates that titration of adsorbed species on the metal cannot be responsible for the high RT dynamic H_2-OSC recorded for the ceria-based samples, which indicates the importance of the support in accepting such spilled over H_2. The linear relationship of this RT H_2-OSC with surface area of the support denotes that storage of H_2 occurs at the surface of the $Ce_{0.68}Zr_{0.32}O_2$ support, the contribution of the titration of adsorbed O_2/H_2 at the surface of the noble metal being negligible. This interpretation is in line with previous studies which suggested that titration of spilled over hydrogen species can be applied to measure surface area of CeO_2 in the proximity of the metal particles (30).

Formation of oxygen vacancies, i.e., so-called irreversible reduction, on exposure to H_2 at RT, was negligible in a Rh/CeO_2 catalyst (21), which is consistent with the above picture of spilling of hydrogen species being the main reaction pathway for the RT H_2-OSC. Detection of water in these experiments highlights that the present process can be defined as OSC. In fact, we observe adsorption and release of the excess of the oxidizing (O_2) or reducing (H_2) agent, which keeps the oxygen partial pressure constant. However, such OSC is not a measure of vacancy creation in the sample, as is often assumed to be the case in OSC measurements. This is an important observation since, at variance with laboratory studies that use a different reducing agent or even no reducing agent, e.g., OBC technique, under real exhaust conditions the oxygen partial pressure is constantly monitored by an oxygen (λ) sensor, and only deviations from the stoichiometric A/F ratio are detected, irrespective of the complex nature of the exhaust mixture or OSC phenomenon. Accordingly, the OSC can be viewed as the ability to buffer the partial oxygen pressure, in which respect the present systems appear to be rather efficient.

The linear relationship of both the spilled H_2 and RT H_2-OSC with surface area deserve some further comments. TPR experiments and oxygen titration of spilled over hydrogen species in NM/CeO_2 systems revealed that 3.9 μmol of H_2 is needed to reduce a BET surface of CeO_2 of 1 m^2, which corresponds to 2 μmol of O_2 titrated (30, 31). The latter value corresponds to 2.4 O nm^{-2} consumed. For comparison 13.1 and 13.5 O nm^{-2} were calculated respectively for CeO_2 and $Ce_{0.68}Zr_{0.32}O_2$ (10). The linear relationships reported in Fig. 3 allows calculation of the amount of H_2 spilled over the PtCeO_2 catalysts as 2.0 and 3.8 μmol of H_2 for a surface area of 1 m^{-2} measured respectively from chemisorption and RT H_2-OSC, assuming the proper stoichiometry for the latter measurement. For Pt/$Ce_{0.68}Zr_{0.32}O_2$, 2.8 and 6.2 μmol of H_2 for a surface area of 1 m^{-2} are obtained respectively from chemisorption and RT H_2-OSC.

The comparison with the above-quoted literature data is interesting since it may suggest that H_2 chemisorption values are lower than would be expected for complete surface coverage. This could be attributed to the sensitivity of H_2 spillover to the experimental conditions which may lead to different amounts of spilled H_2 according to the pretreatment and experimental conditions (16, 18, 19). Clearly, while a linear relationship is generally detected, the absolute values of the adsorbed or consumed H_2 or O_2 per square meter of CeO_2 surface critically depend on the experimental setup. Consistently, several authors found a linear relationship between the amount of H_2 consumed and "surface" reduction in TPR experiments (32–35); none of these, however, could be related to a precise surface geometry of the CeO_2 particle (36). The values obtained on the Pt/$Ce_{0.68}Zr_{0.32}O_2$ catalysts are in line with such an interpretation since a different response of the system to the experimental condition may be expected in the CZ system compared with CeO_2 one. Even though these results were obtained under specific experimental conditions employed here, a possible corollary of the present observation would be that the insertion of ZrO_2 into CeO_2 promotes the spillover capacity of CeO_2.

The key to the RT H_2-OSC is the ability of the metal to dissociate H_2. This is clearly demonstrated in experiments involving Pt/CeZr samples of 100 and 77 m^2 g^{-1}. Dynamic OSC measurements conducted on these samples after the cleaning procedure, when the metal would be fully oxidized, resulted in negligible RT OSC; prior reduction is necessary. After the more severe aging procedures, a specific reduction step is not necessary, as the metals are more difficult to oxidize and would not exist as polycrystalline oxides. During dynamic measurements, the ease of oxidation of ceria-based material means that the support (or at least its surface) is oxidized largely *in situ*, and the metal is simply passivated. In fact, the main difference between the reduced (pretreatment C) and reduced/passivated (pretreatment D) samples in these experiments is that the former shows low H_2 uptake on the first pulse (data not shown). Once an O_2 pulse has been made, the surface is titrated of adsorbed H_2 and/or oxidized and thereafter the behavior observed is the same.

It should be noted that quantitative comparison of the dynamic H_2-OSC and chemisorption results reveals a higher measured H_2 uptake in the former. Two explanations may be put forward for this observation. The first stems from

the fact that H_2O is formed *in situ* in dynamic H_2-OSC measurements. As H_2O is known to promote spillover, any retained on the surface could increase spillover relative to chemisorption measurements. The second is that, as outlined in an earlier publication (15) and above, significant differences in uptake may be observed due to the very different conditions of adsorption, higher uptake being observed due to the higher H_2 pressure of the dynamic experiments. The higher uptake at 20 Torr in the chemisorption data reported here is also suggestive of this phenomenon. The dynamics of H_2 spillover certainly play an important role in the experiment. In fact a reduced physical mixture of equivalent amounts of PtAl1 and $Ce_{0.68}Zr_{0.32}O_2$ showed appreciable H_2-OSC at RT (2.2 ml g^{-1}), which increased to 4.8 ml g^{-1} at 373 K. No H_2-OSC was detected on pure $Ce_{0.68}Zr_{0.32}O_2$ under such conditions. This is an interesting observation since it shows that long-range migration phenomena occur under these very mild conditions, hydrogen not being spilled only over the CeO_2 particles in close contact with the noble metal (30).

While PtCeZr1 and PdCeZr1 samples show comparable dynamic OSC behavior at RT, a smaller value was obtained for RhCeZr1. After redox-aging, a difference between Rh and the other two metals persists. A clear explanation for this observation is difficult on the basis of the data available. The similarities of the surface areas indicate that this should not be a factor, and the data could be taken to indicate that there is a difference in spillover efficiency under the experimental conditions employed. Chemisorption experiments at 298 K indicate that similar uptake is achieved in a shorter time in the case of the Rh sample. The Rh sample has a dispersion similar to that of Pt but a slightly higher loading, which may partly explain the difference in equilibration time. Likewise it should considered that at comparable metal loading the Rh catalyst has more than twice the number of Rh atoms. However, as already mentioned, spillover is sensitive to experimental conditions and the nature of the catalyst, making straightforward comparison of data sometimes difficult. Further work is needed to fully elucidate this point.

4.1.2. H_2-OSC at higher temperatures. For the high-surface-area ceria–zirconia samples, moderate increases in H_2 and O_2 uptake are observed between RT and 773 K (Table 3). While vacancy creation is unlikely to be a factor at RT, it is certainly a contributing factor at higher temperatures. However, spillover may also be a factor as it is an activated process (37). In fact, we have previously demonstrated that there is substantial reversible H_2 adsorption on a reduced $Rh/Ce_{0.6}Zr_{0.4}O_2$ sample, part of the stored hydrogen being retained reversibly at the surface up to approximately 600 K (15). In addition, the results obtained for the physical mixture indicate that spillover is important at all temperature, if the support has the ability to accept spilled over hydrogen. Thus, *in situ* reduction at high-temperature reduction may lead to such H_2 retention. The relative importance of spillover and reduction should show a temperature dependence. Factors such as desorption between pulses (and therefore the time between pulses) may become critical to the results obtained. However, it is not possible to discriminate between H_2 adsorbed and reacted on the basis of O_2 uptake as the stoichiometries of the vacancy creation and titration reactions are the same. Thus, the possibility exists that the values obtained at higher temperatures may be a mixture of vacancy reoxidation and titration. This general observation may be applied to CeO_2- and CeO_2/ZrO_2-based samples, but the latter exhibits higher spillover and textural stability, potentially making the spillover contribution more significant.

For the CeO_2/ZrO_2 samples obtained after pretreatment B (redox-aging), H_2 and O_2 uptake values increase significantly across the temperature range and become larger than in the case of the high-surface-area samples. The most likely explanation of this observation is that the improved redox behavior of ceria–zirconia materials during TPR may be reproduced under dynamic conditions. Although, as outlined above, the relative importance of spillover and reduction could not be ascertained, the surface areas of the recycled samples are definitely smaller and, as indicated above, at RT spillover is not greater than for the high-surface-area samples. Thus, on increasing the temperature, a more significant contribution to the H_2-OSC via an oxygen vacancy creation mechanism is likely. Remarkably, under the present conditions, the dynamic H_2-OSC behavior exhibited for the 15 and 7 m^2 g^{-1} samples at the higher temperatures (where vacancy creation should become more important) is similar to that of the 100 m^2 g^{-1} sample (respectively 8.8, 9.0, and 8.9 ml O_2 g^{-1} at 773 K), while that of the redox-aged (30 m^2 g^{-1}) sample is in fact improved (11.6 ml O_2 g^{-1} at 773 K).

There is a notable difference between the PtCeZr and PtCe materials on increasing the temperature of dynamic H_2-OSC measurements. Unlike PtCeZr, for each PtCe sample there is a low and almost constant uptake across the temperatures investigated. In fact there appears to be a maximum in the uptakes observed between 373 and 473 K. In addition, at all temperatures, the values obtained for PtCe samples decrease with decreasing surface area. This not only indicates the enhanced redox behavior of ceria–zirconia relative to ceria under dynamic conditions, but also suggests that under our dynamic conditions redox processes in PtCe are limited to the surface, independently of whether a spillover- or vacancy creation-related redox mechanism is operating.

4.2. Dynamic OSC Using CO

Dynamic CO-OSC has been subject of recent studies (10, 11, 38, 39). Generally speaking, insertion of ZrO_2 into the CeO_2 lattice increased the CO-OSC of CeO_2, particularly

under transient conditions. The most effective CO-OSC is observed with CeO_2–ZrO_2 mixed oxides slightly enriched in CeO_2. This is due to the fact that, while the dynamics of the reduction and oxidation appear most rapid at the ZrO_2-rich side (11, 14), a substantial amount of the reducible CeO_2 moiety is needed to obtain the best performance (10, 11). This qualitatively reflects the redox behavior when H_2 is used as reducing agent, in that it was previously suggested that large ZrO_2 amounts improve the reduction behavior, as long as a cubic type of cation lattice is retained, e.g., t" and c phases (4, 17) The aim of this work is to compare the influence of the reducing agent on the transient redox of the NM/CeO_2–ZrO_2; accordingly only the relevant aspects are considered.

The most important finding is that CO-OSC becomes appreciable only at high temperatures where oxygen vacancy creation is likely to occur. The absence of significant CO_2 formation at RT indicates that the observed RT H_2-OSC is related to the ability of the $Ce_{0.68}Zr_{0.32}O_2$ to spill hydrogen species, rather than to migration of oxygen. In fact, the mobility of oxygen species over the ceria surface is very effective at high temperatures; however, at low temperatures migration of hydrogen species is much faster (40).

The sensitivity of CO-OSC to the pretreatment of the catalyst is an indication that subtle and complex phenomena occur as a consequence of the interaction of CO with the CeO_2 surface. In the reduced state, and particularly at low temperatures, significant CO storage effects have been detected. These phenomena include CO adsorption and dissociation, as detected by evolution of CO and CO_2 under the oxygen pulse. More importantly, long reaction times are needed to reach stationary conditions when high-surface-area sample is investigated. Once again, these experiments underline the critical importance of defining standard pre-treatment/cleaning conditions to allow comparison of data between different catalysts. Very often indeed, CO-OSC has been measured using a few pulses or using a TCD detector; under such conditions such phenomena may easily be overlooked. However, when the catalyst is simply preoxidized, CO dissociation is depressed. In fact this dissociation is related to the powerful ability of reduced CeO_2 moieties to easily extract oxygen from small molecules containing oxygen such as H_2O, CO_2, NO, and N_2O (41–44). However, this is not the complete simple picture, since we observed significant CO dissociation even after pulsing a large excess of O_2 over the catalyst, which should result in complete reoxidation of the reduced $Ce_{0.68}Zr_{0.32}O_2$ moiety (14). We believe that accumulation of CO-derived species, either surface carbon or carbonates (24, 25), may hinder to some extent the reoxidation of the reduced catalyst due to the difficulty of desorption of such species. The presence of oxygen vacancies in the bulk of the mixed oxides would then provide the additional driving force for further CO dissociation, as has been previously suggested for CeO_2-based catalysts (45). By increasing the temperature, progressive desorption of adsorbed CO-derived species occurs, leading to annihilation of bulk oxygen vacancies, thus fully reoxidizing the catalyst (46).

At variance with H_2 as reducing agent (at high temperatures), CO-OSC is strongly dependent on the extent of surface area, which is a strong indication that the reduction mechanism strongly depends on the nature of the reducing agent. Surface reaction was suggested to be rate limiting in the reduction process when CO is employed as reducing agent (38), even though recent evidence suggests that at low temperatures oxygen mobility in the bulk of the CeO_2–ZrO_2 mixed oxide may affect the rate of reduction (11). As far as H_2 is concerned, the situation appears somewhat complex, since several factors, e.g., structural, textural, and even preparation method, heavily affected the reduction behavior of the CeO_2–ZrO_2 mixed oxides (4). However, by using a H_2/D_2 mixture it was possible to show that the rate-limiting step in the reduction process changes with temperature: a kinetic isotopic effect was observed only above 700–800 K (47), suggesting that surface processes are rate-limiting above these temperatures. Accordingly, it appears reasonable that in the range of the temperatures investigated here, modification of bulk properties of the mixed oxide may affect its reduction behavior, as previously observed (8, 9), leading to the otherwise unexpected result of a higher efficiency of H_2-OSC in the redox-aged, i.e., sintered, NM/$Ce_{0.68}Zr_{0.32}O_2$.

5. CONCLUSIONS

Comparison of H_2 and CO in dynamic OSC measurements revealed that the mechanism of OSC is strongly dependent on the nature of the reducing agent. At RT and using H_2 as the reducing agent, the ability of ceria/zirconia to accept spilled hydrogen allows these materials to act as effective OSC systems. Hydrogen is spilled under the reducing conditions and, later on, titrated by oxygen during the oxidizing part of the cycle. As a result, the system behaves as an effective oxygen buffer device, without any significant involvement of lattice oxygen from the support. This contrasts with the high-temperature behavior. Under the latter conditions, in effect, the operating mechanism consists of creating oxygen vacancies during the reducing part of the cycle, which are later replenished on switching the surrounding atmosphere to net oxidizing conditions. For intermediate temperatures, the overall OSC behavior would result from a significant contribution of the two mechanisms. Retention and high reactivity of hydrogen species on the surface are particularly interesting in view of recent findings that, using H_2 as reducing agent, selective catalytic NO_x reduction can be achieved over Pt catalysts even in excess O_2 (48, 49).

Vacancy creation is the traditionally proposed mechanism by which CO interacts with CeO_2-based systems. However, even for this reducing agent, an appreciable contribution from processes in addition to vacancy creation was detected, particularly on the reduced surface, indicating that several phenomenona may contribute to the dynamic OSC property.

ACKNOWLEDGMENTS

The present paper has received financial support from the TMR Program of the European Commission (Contract FMRX-CT-96-0060). Financial support from the University of Trieste, Regione Friuli Venezia-Giulia, Fondo regionale per la Ricerca L.R. 3/1998, MURST Programmi di Ricerca Scientifica di Rilevante Interesse Nazionale—1988, Fondo Trieste 1999, the CICYT (Contract MAT99-0570), and the Junta de Andalucía is also acknowledged.

REFERENCES

1. Taylor, K. C., *in* "Catalysis—Science and Technology" (J. R. Anderson and M. Boudart, Eds.), Chap. 2, pp. 119–170. Springer-Verlag, Berlin, 1984.
2. Yao, H. C., and Yu Yao, Y. F., *J. Catal.* **86**, 254 (1984).
3. Heck, R. M., and Farrauto, R. J., "Catalytic Air Pollution Control: Commercial Technology" Van Nostrand Reinhold, New York, 1995.
4. Kaspar, J., Fornasiero, P., and Graziani, M., *Catal. Today* **50**, 285 (1999).
5. Hickey, N., Fornasiero, P., Kaspar, J., Graziani, M., Blanco, G., and Bernal, S., *Chem. Commun.*, 357 (2000).
6. Trovarelli, A., *Catal. Rev.-Sci. Eng.* **38**, 439 (1996).
7. Bernal, S., Blanco, G., Cauqui, M. A., Corchado, P., Pintado, J. M., and Rodriguez-Izquierdo, J. M., *Chem. Commun.*, 1545 (1997).
8. Fornasiero, P., Balducci, G., Di Monte, R., Kaspar, J., Sergo, V., Gubitosa, G., Ferrero, A., and Graziani, M., *J. Catal.* **164**, 173 (1996).
9. Izu, N., Omata, T., and Otsuka-Yao-Matsuo, S., *J. Alloys Compd.* **270**, 107 (1998).
10. Madier, Y., Descorme, C., LeGovic, A. M., and Duprez, D., *J. Phys. Chem. B* **103**, 10999 (1999).
11. Boaro, M., de Leitenburg, C., Dolcetti, G., and Trovarelli, A., *J. Catal.* **193**, 338 (2000).
12. Colon, G., Pijolat, M., Valdivieso, F., Vidal, H., Kaspar, J., Finocchio, E., Daturi, M., Binet, C., Lavalley, J. C., Baker, R. T., and Bernal, S., *J. Chem. Soc. Faraday Trans.* **94**, 3717 (1998).
13. Daturi, M., Binet, C., Lavalley, J. C., Vidal, H., Kaspar, J., Graziani, M., and Blanchard, G., *J. Chim. Phys.* **95**, 2048 (1998).
14. Vidal, H., Kaspar, J., Pijolat, M., Colon, G., Bernal, S., Cordon, A. M., Perrichon, V., and Fally, F., *Appl. Catal. B* **27**, 49 (2000).
15. Fornasiero, P., Hickey, N., Kaspar, J., Dossi, C., Gava, D., and Graziani, M., *J. Catal.* **189**, 326 (2000).
16. Gatica, J. M., Baker, R. T., Fornasiero, P., Bernal, S., Blanco, G., and Kaspar, J., *J. Phys. Chem. B* **104**, 4667 (2000).
17. Fornasiero, P., Di Monte, R., Ranga Rao, G., Kaspar, J., Meriani, S., Trovarelli, A., and Graziani, M., *J. Catal.* **151**, 168 (1995).
18. Bernal, S., Calvino, J. J., Cifredo, G. A., Laachir, A., Perrichon, V., and Herrmann, J. M., *Langmuir* **10**, 717 (1994).
19. Fornasiero, P., Kaspar, J., Sergo, V., and Graziani, M., *J. Catal.* **182**, 56 (1999).
20. Lieske, H., Lietz, G., Spindler, H., and Voelter, J., *J. Catal.* **81**, 8 (1983).
21. Bernal, S., Calvino, J. J., Cifredo, G. A., Rodriguez-Izquierdo, J. M., Perrichon, V., and Laachir, A., *J. Catal.* **137**, 1 (1992).
22. Perrichon, V., Laachir, A., Abouarnadasse, S., Touret, O., and Blanchard, G., *Appl. Catal. A* **129**, 69 (1995).
23. Bernal, S., Calvino, J. J., Cauqui, M. A., Gatica, J. M., Larese, C., Omil, J. A. P., and Pintado, J. M., *Catal. Today* **50**, 175 (1999).
24. Li, C., Domen, K., Maruya, K., and Onishi, T., *J. Chem. Soc. Chem. Commun.*, 1541 (1988).
25. Li, C., Sakata, Y., Arai, T., Domen, K., Maruya, K., and Onishi, T., *J. Chem. Soc. Faraday Trans. I* **85**, 929 (1989).
26. Mullins, D. R., and Overbury, S. H., *J. Catal.* **188**, 340 (1999).
27. Serre, C., Garin, F., Belot, G., and Maire, G., *J. Catal.* **141**, 1 (1993).
28. Holmgren, A., Andersson, B., and Duprez, D., *Appl. Catal. B* **22**, 215 (1999).
29. van't Blik, H. F. J., van Zon, J. B. A. D., Huizinga, T., Vis, J. C., Koningsberger, D. C., and Prins, R., *J. Am. Chem. Soc.* **107**, 3139 (1985).
30. Salasc, S., Perrichon, V., Primet, M., Chevrier, M., and Mouaddib-Moral, N., *J. Catal.* **189**, 401 (2000).
31. Rogemond, E., Frety, R., Perrichon, V., Primet, M., Salasc, S., Chevrier, M., Gauthier, C., and Mathis, F., *J. Catal.* **169**, 120 (1997).
32. Bruce, L. A., Hoang, M., Hughes, A. E., and Turner, T. W., *Appl. Catal. A* **134**, 351 (1996).
33. Johnson, M. F. L., and Mooi, J., *J. Catal.* **103**, 502 (1987).
34. Laachir, A., Perrichon, V., Badri, A., Lamotte, J., Catherine, E., Lavalley, J. C., El Fallah, J., Hilaire, L., Le Normand, F., Quemere, E., Sauvion, N. S., and Touret, O., *J. Chem. Soc. Faraday Trans.* **87**, 1601 (1991).
35. Perrichon, V., Laachir, A., Bergeret, G., Frety, R., Tournayan, L., and Touret, O., *J. Chem. Soc. Faraday Trans.* **90**, 773 (1994).
36. Kaspar, J., Graziani, M., and Fornasiero, P., *in* "Handbook on the Physics and Chemistry of Rare Earths: The Role of Rare Earths in Catalysis." (K. A. Gschneidner, Jr., and L. Eyring, Eds.), Chap. 184, pp. 159–267. Elsevier Science, Amsterdam, 2000.
37. Conner, W. C., Jr., Pajonk, G. M., and Teichner, S. J., *in* "Spillover of Sorbed Species" (D. D. Eley, H. Pines, and P. B. Weisz, Eds.), *Advances in Catalysis,* Vol. 34, pp. 1–79, Academic Press, Orlando, FL, 1986.
38. Hori, C. E., Permana, H., Ng, K. Y. S., Brenner, A., More, K., Rahmoeller, K. M., and Belton, D. N., *Appl. Catal. B* **16**, 105 (1998).
39. Hori, C. E., Brenner, A., Ng, K. Y. S., Rahmoeller, K. M., and Belton, D., *Catal. Today* **50**, 299 (1999).
40. Martin, D., and Duprez, D., *Stud. Surf. Sci. Catal.* **77**, 201 (1993).
41. Padeste, C., Cant, N. W., and Trimm, D. L., *Catal. Lett.* **18**, 305 (1993).
42. Ranga Rao, G., Kaspar, J., Di Monte, R., Meriani, S., and Graziani, M., *Catal. Lett.* **24**, 107 (1994).
43. Otsuka, K., Hatano, M., and Morikawa, A., *J. Catal.* **79**, 493 (1983).
44. Trovarelli, A., Dolcetti, G., de Leitenburg, C., Kaspar, J., Finetti, P., and Santoni, A., *J. Chem. Soc. Faraday Trans.* **88**, 1311 (1992).
45. Serre, C., Garin, F., Belot, G., and Maire, G., *J. Catal.* **141**, 9 (1993).
46. de Leitenburg, C., Trovarelli, A., and Kaspar, J., *J. Catal.* **166**, 98 (1997).
47. Fornasiero, P., Kaspar, J., and Graziani, M., *Appl. Catal. B* **22**, L11 (1999).
48. Burch, R., Shestov, A. A., and Sullivan, J. A., *J. Catal.* **188**, 69 (1999).
49. Burch, R., and Coleman, M. D., *Appl. Catal. B* **23**, 115 (1999).